Optics Letters

Narrowband carrier-envelope phase stable mid-infrared pulses at wavelengths beyond 10 μm by chirped-pulse difference frequency generation

A. Cartella,[1] T. F. Nova,[1,2] A. Oriana,[3] G. Cerullo,[3] M. Först,[1] C. Manzoni,[3] and A. Cavalleri[1,2,4,*]

[1]Max Planck Institute for the Structure and Dynamics of Matter, Hamburg, Germany
[2]The Hamburg Centre for Ultrafast Imaging, Hamburg, Germany
[3]IFN-CNR, Dipartimento di Fisica—Politecnico di Milano, Milan, Italy
[4]Department of Physics, Clarendon Laboratory, University of Oxford, Oxford, UK
*Corresponding author: andrea.cavalleri@mpsd.mpg.de

Received 8 November 2016; revised 29 December 2016; accepted 9 January 2017; posted 10 January 2017 (Doc. ID 280460); published 3 February 2017

We report on the generation of narrowband carrier-envelope phase stable mid-infrared (MIR) pulses between 10 and 15 μm. High pulse energies and narrow bandwidths are required for the selective nonlinear excitation of collective modes of matter that is not possible with current sources. We demonstrate bandwidths of <2% at 12.5 μm wavelength through difference frequency generation between two near-infrared (NIR) pulses, which are linearly chirped. We obtain a reduction in bandwidth by one order of magnitude, compared to schemes that make use of transform-limited NIR pulses. The wavelength of the narrowband MIR pulse can be tuned by changing the optical delay between the two chirped NIR pulses.

OCIS codes: (190.7110) Ultrafast nonlinear optics; (300.6250) Spectroscopy, condensed matter; (190.4410) Nonlinear optics, parametric processes.

https://doi.org/10.1364/OL.42.000663

Optical pulses at mid-infrared (MIR) frequencies (6–20 μm wavelength) are a powerful tool to control the functional properties of solids and molecular systems [1,2], for example, by driving lattice vibrations to large amplitudes [3,4]. Typically, tunable MIR pulses between 10 and 20 μm are obtained by difference frequency generation (DFG) between two femtosecond near-infrared (NIR) pulses [5,6]. However, the broad bandwidths of the NIR pulses that are used in these cases translate into MIR pulses with relative bandwidths of 10%–30% $\Delta\omega/\omega_0$. These are much larger than the vibrational mode linewidths in condensed matter, which are often of the order of a few percent only, resulting in poor spectral selectivity of the excitation. In order to selectively access such modes and, in particular, to separately drive closely spaced modes, it is necessary to reduce the MIR bandwidth by at least one order of magnitude.

The most straightforward method to reduce the bandwidth of either the interacting NIR pulses or of the resulting MIR light consists of linear spectral filtering by bandpass filters (such as Fabry–Perot filters) or by slits placed in the Fourier plane of a zero-dispersion pulse shaper [7]. However, this approach is intrinsically inefficient, since its energy loss is proportional to the achieved spectral narrowing. Narrowband pulses can be efficiently generated by nonlinear interaction between suitably chirped broadband pulses, allowing for frequency components with the same sum or difference to interact and directly transfer their energy into the narrowband output. This approach has been successfully applied in various spectral regions: narrowband visible pulses have been obtained via sum frequency generation of NIR pulses with opposite chirp [8]. Analogously, narrowband MIR pulses with wavelengths shorter than 10 μm have been generated by DFG between NIR pulses having chirp with the same sign [9–11]. However, the spectral region between 10 and 20 μm, of interest for vibrational control in solids, has not been addressed.

Furthermore, the narrowband MIR pulses generated so far were lacking CEP stability, a feature shown only in the THz range, at 300 μm wavelength [12]. However, this CEP stability is a big asset for the investigation of mid-infrared and THz vibrational control in condensed matter as it enables to explore the coherent perturbation of electronic, magnetic, or structural degrees of freedom on the sub-cycle phonon timescale [13], as well as phase-dependent effects [14].

In this Letter, we apply chirped-pulse DFG to generate narrowband, CEP-stable MIR pulses in the 10–15 μm wavelength range. We achieve pulses with relative bandwidths of $\Delta\omega/\omega_0 = 1.6\%$ at a 12.5 μm wavelength, one order of magnitude narrower than the bandwidth obtained from the unchirped NIR pulses.

The MIR carrier wavelength is easily tuned by changing the delay between the chirped NIR pulses.

Figure 1 summarizes the principle of narrowband MIR pulse generation by DFG among chirped pulses. Panels (a)–(c) show the time-frequency Wigner distributions [15] of the interacting NIR pulses; the MIR light is generated at the difference frequency (DF) between frequency components interacting at the same time in the nonlinear medium. The MIR bandwidth can be estimated at the zero order as $\Delta\Omega = \Omega_2 - \Omega_1$ where $\Omega_{1/2}$ is the frequency difference between the closest/farthest interacting frequency components. If the two NIR pulses are transform limited, all their spectral components interact simultaneously [see Fig. 1(a)], giving rise to the broadest MIR pulse [dotted line in Fig. 1(d)]. If the two NIR pulses are linearly chirped with different group delay dispersion (GDD), as depicted in Fig. 1(b), only a subset of their frequency components can interact, leading to a decrease in the MIR bandwidth [dashed line in Fig. 1(d)]. In this case, the NIR chirped pulses can be described as $E_{1,2}(t) = E_{01,02}(t)\exp[i(\omega_{1,2}t + C_{1,2}t^2)]$, where $E_{01,02}(t)$ is the envelope and $C_{1,2}$ is the linear chirp. The resulting MIR pulses are then

$$E_{\mathrm{MIR}}(t) = E_{01}(t)E_{02}^{*}(t)\exp[i(\omega_1 - \omega_2)t + i(C_1 - C_2)t^2].$$

Since the chirp in the two pulses is different, $C_1 \neq C_2$, the MIR pulses acquire a time-dependent frequency, i.e., they are also chirped. Furthermore, if the two NIR pulses have the same bandwidths, this also implies that some of the frequency components of the most dispersed pulse do not interact with the other, resulting in a strong reduction of the DFG efficiency.

If the two NIR pulses are chirped with the same amount of GDD [see Fig. 1(c)], $C_1 = C_2$ and the spectral components involved in the DFG process are all at constant beat note; hence $\Delta\Omega = \Omega_2 - \Omega_1 \approx 0$. This potentially leads to the generation of the narrowest, almost monochromatic MIR pulse. However, the DF spectrum gets inevitably broadened, since any cut at time t' of the time-frequency distribution of the NIR pulses has a finite bandwidth. A first-order estimation of the MIR bandwidth $\Delta\omega$ [solid line in Fig. 1(d)] can be obtained by recalling that the MIR pulse cannot be longer than the interacting stretched NIR pulses. For this reason, fixing $\Delta\omega$ corresponds to choosing the target MIR duration and, hence, the NIR stretching.

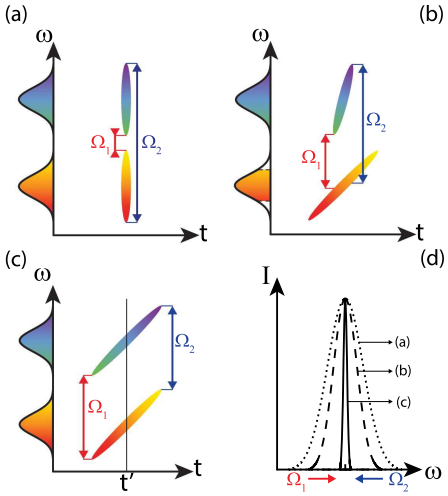

Fig. 1. Principle of the narrowband MIR pulse generation: (a)–(c) time-frequency Wigner distributions of the interacting NIR pulses for various chirp configurations; the MIR components are generated at the DF between NIR spectral frequencies at the same time delay. Ω_1 and Ω_2 are the lowest and highest MIR frequencies, respectively. (d) Corresponding MIR spectra. When going from the configuration (a)–(c), Ω_1 and Ω_2 get closer to each other, resulting in a narrower MIR spectrum.

The experimental setup for the generation of narrowband MIR pulses is illustrated in Fig. 2. The NIR pulses were obtained from two-stage optical parametric amplifiers (OPAs), pumped with 100 fs, 800 nm pulses from a commercial Ti:sapphire regenerative amplifier at a 1 kHz repetition rate. The two OPAs were seeded by the same white light continuum; hence, they possess the same CEP fluctuations in their signal output pulses [16]. The MIR pulses generated by DFG are thus CEP stable [16–18], making it possible to measure their electric fields by EOS [5]. To this end, we used 20 fs gate pulses at a 900 nm wavelength, derived from a synchronized non-collinear OPA [19].

The NIR pulses were tuned to 1.31 (~229 THz) and 1.46 μm (~205 THz), with pulse energies of 330 and 310 μJ, respectively. These were made to interact in a 600 μm thick GaSe crystal to generate MIR pulses at 12.5 μm (24 THz). At this wavelength, $\Delta\omega/\omega_0 \approx 2\%$ corresponds to a pulse duration of about 1 ps, setting a lower limit for the duration of the chirped NIR pulses. The NIR wavelengths were tuned to above 1.2 μm to prevent two-photon absorption in GaSe.

The NIR pulses were chirped by linear propagation in highly dispersive transparent materials, which are far simpler to handle than gratings [8,9] or prism pairs [11], and introduce an easily reproducible dispersion. They are also easily inserted or removed from the optical setup to switch between the broadband and narrowband generation schemes, without affecting the footprint or the alignment. These materials should be transparent in the NIR, with a high enough dispersion to stretch the OPA pulses in a contained space. They should introduce suitable GDD and third-order dispersion (TOD), allowing for the matching of the two NIR chirps, and have a high bandgap to prevent two-photon absorption. In Table 1, we show the calculated GDD and TOD for three readily available materials commonly used in the NIR: zinc selenide (ZnSe), cadmium telluride (CdTe), and silicon (Si). For any of these materials, rods of different thicknesses L_I and L_{II} are required to obtain the same GDD for the two different OPA frequencies, respectively. Once L_I and L_{II} are set, the material with the optimum dispersion properties is the one for which TOD_I and TOD_{II} are closest to each other, making $\mathrm{TOD}_I/\mathrm{TOD}_{II}$ a good figure of merit.

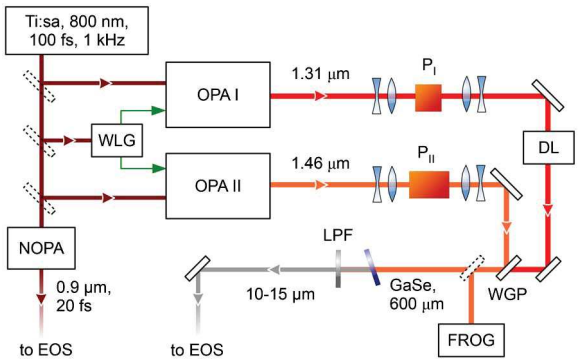

Fig. 2. Setup for the generation of the MIR pulses. OPA I/II, two-stage IR OPAs; WLG, white light generation; DL, delay line; $P_{I/II}$, ZnSe rods; WGP, wire grid polarizer; LPF, long pass filter; NOPA, non-collinear OPA.

Table 1. Dispersion at the Pump (λ_I) and Signal (λ_{II}) Wavelengths Introduced by Propagation in 1 cm of Highly Dispersive Materials[a]

	$\lambda_I = 1.31\ \mu$m		$\lambda_{II} = 1.46\ \mu$m		
Material	GDD_I/L[fs^2/cm]	TOD_I/L[fs^3/cm]	GDD_{II}/L[fs^2/cm]	TOD_{II}/L[fs^3/cm]	TOD_I/TOD_{II}
ZnSe	4741	4277	4131	3992	0.93
CdTe	10530	11500	8938	10080	0.96
Si	16865	60530	12330	17320	2.55

[a]The last column is the ratio between the TOD_I and TOD_{II} at plate thicknesses where $GDD_I = GDD_{II}$. The dispersion was calculated with Sellmeier coefficients from [20–22].

Table 1 shows that ZnSe and CdTe are very similar from this point of view, while Si is significantly worse. We chose ZnSe as a dispersive element because of its smaller nonlinear refractive index, and because of its higher bandgap (2.8 versus 1.5 eV in CdTe) which minimizes two-photon absorption [23]. ZnSe rods of $L_I = 4.7$ cm and $L_{II} = 5.2$ cm thickness were used to obtain GDD of about 22, 500 fs^2, which chirps the 60 fs NIR pulses to ≈1 ps. The amount of dispersion could be easily doubled to GDD = 45, 000 fs^2 by introducing two ZnSe rods into each NIR beam.

Spectral broadening due to self-phase modulation was minimized by decreasing the intensities of the two NIR beams with two telescopes. The beams were magnified from 4 to 10 mm (FWHM) before chirping and demagnified again to 4 mm onto the DFG crystal. The overall throughput of the stretching section was 85% (73%) when we introduced one (two) ZnSe plate(s) per beam.

Figure 3 displays the time-frequency Wigner map of the NIR pulses before (a) and after (b) stretching with one ZnSe rod, retrieved from frequency-resolved optical gating (FROG) measurements [24]. Without the stretching blocks [see panel (a)], both OPA NIR pulses were transform limited, with a duration of 60 fs. Their DFG produced broadband MIR pulses at 24 THz (12.5 μm) with 4.2 μJ of energy and $\Delta\omega/\omega_0 = 15\%$ bandwidth, as shown by the black dotted line spectrum in Fig. 4(b), calculated as the Fourier transform of the measured EOS trace [black line in Fig. 4(a)]. Figure 3(b) shows the Wigner map of the stretched NIR pulses after inserting the ZnSe rods of thickness L_I and L_{II}. As expected, the time-frequency traces of both NIR pulses are parallel to each other and to the dashed line, which represents the frequency chirp with GDD = 22, 500 fs^2 and TOD = 20, 000 fs^3.

Figure 4(a) shows the CEP-stable MIR pulses generated by DFG in the GaSe crystal and measured by EOS. Stretching the NIR pulses by one or two pairs of ZnSe rods results in an increase in MIR pulse duration from 0.12 to 0.92 and 1.65 ps, concomitant with a bandwidth reduction from 15% $\Delta\omega/\omega_0$ to 2.5% and 1.6% $\Delta\omega/\omega_0$, respectively, as shown in Fig. 4(b). The time-bandwidth product, close to 0.44 for the 0.12-ps broadband MIR pulses, only slightly increased to 0.55 (one rod pair) and 0.63 (two rod pairs).

Stretching the two NIR pulses also caused a reduction of the MIR pulse energy to 1.4 and 0.6 μJ, respectively. We attribute this efficiency reduction mostly to the lower peak intensity of the chirped NIR pulses in the DFG process, with a minor contribution due to the losses in stretching sections.

The two stretching steps reduced the bandwidth to 16% and 10% of the starting value, respectively. For spectral filtering techniques, this corresponds to the maximum theoretical energy efficiency, without keeping into account further losses introduced by the optical elements. In our case, the energy efficiency was 35% and 15%, and can potentially be increased by the use of a thicker GaSe crystal or focused NIR beams.

The MIR beam radius in the focus was estimated to be around 50 μm, obtained by measuring the transmission

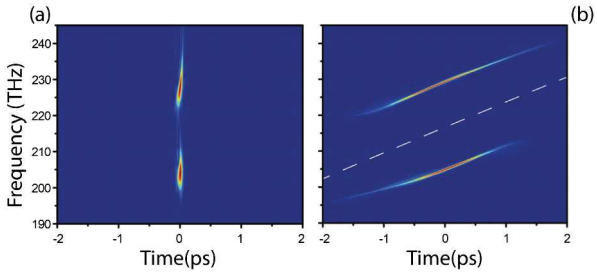

Fig. 3. Experimental time-frequency Wigner maps of the NIR OPA pulses, retrieved from the measured SHG-FROG. (a) Pulses as generated (close to the transform limit). (b) Pulses chirped by one ZnSe plate in each optical path. Dashed line: the target spectral chirp with GDD = 22, 500 fs^2 and TOD = 20, 000 fs^3.

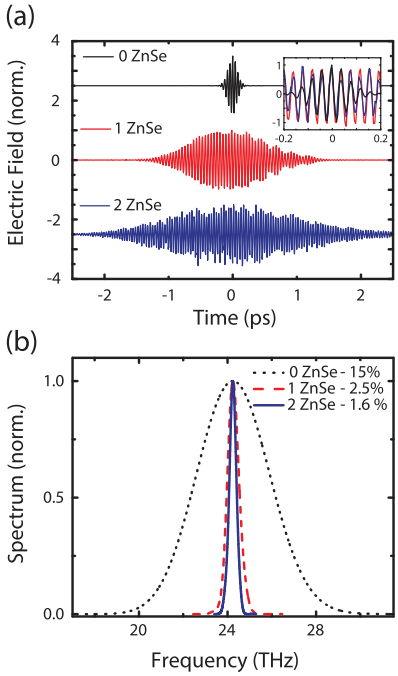

Fig. 4. Normalized EOS (a) traces and (b) spectra of the MIR pulses for different amounts of the NIR chirp. The data in panel (a) are offset for clarity, and the inset shows the EOS traces around 0 ps. The percentage in the legend of panel (b) indicates the relative bandwidth $\Delta\omega/\omega_0$.

through a calibrated 75 μm pinhole. This value was constant for all the measurements, indicating that the beam quality is not affected by the NIR stretching setup. For the 0.6 μJ, 1.65 ps pulses discussed above, this corresponds to a 1.9 MV/cm peak electric field.

Delay-dependent frequency tuning of the MIR output is reported in Fig. 5(c), where the red and blue solid lines depict the narrow spectra obtained for different NIR pulse delays (with one ZnSe rod pair), rescaled according to the corresponding measured energy and normalized to the maximum pulse energy (1.4 μJ). Indeed, if the delay between the incoming pulses is changed, the subset of frequencies that can interact at any time t' in the DFG is shifted and, hence, their difference frequency changes [11]. In addition, the pulse energy of the narrowband MIR light scales with the shape of the broadband spectrum (black line) because changing the NIR pulse delay affects the amount of interacting frequency components.

An illustrative example is shown in Fig. 5(a), where the delay between the NIR pulses is such that only the frequencies close to each other (red arrow) interact. Since the chirp of the NIR pulses is still the same, the narrow MIR bandwidth remains, but the central frequency is $\Omega_{\mathrm{MIR},1}$, on the low-frequency region of the corresponding broadband pulse. Similarly, Fig. 5(b) shows the situation where the pulse delay only allows for the interaction of the NIR frequency components farther from each other (blue arrow), resulting in the $\Omega_{\mathrm{MIR},2}$ central wavelength, on the high-frequency wing of the corresponding broadband pulse.

Tunability of the MIR source can be also be obtained by tuning the OPA wavelengths, allowing us to optimize the conversion even at longer MIR wavelengths. In this case, by tuning each OPA by ±4 THz around the center wavelengths ($\lambda_I = 1.31$ μm and $\lambda_{II} = 1.46$ μm), the GDD of each beam varies only by $\Delta\mathrm{GDD} \approx \mathrm{TOD} * \Delta\omega \approx 150$ fs^2. Hence, thanks to the dispersion properties of ZnSe, the chirps of the two NIR beams are still matched, preserving narrowband interaction. The only factor limiting the MIR tunability is the phonon absorption in the GaSe crystal above 17 μm. Even longer wavelengths could then be achieved by applying this technique to organic crystals as a nonlinear medium [25].

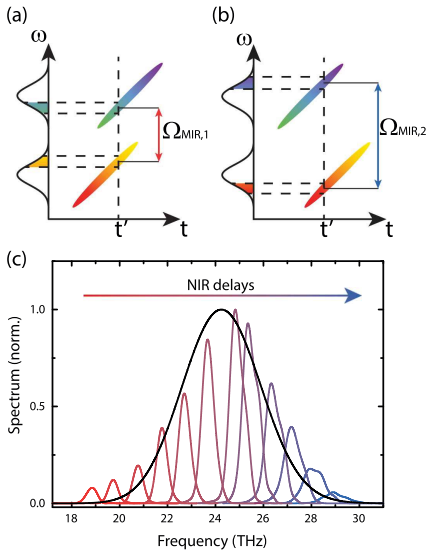

Fig. 5. Delay-dependent frequency tuning. NIR pulse delays that allow for the interaction of the (a) closest and (b) farthest frequency components. (c) Black line: spectrum of the broadband MIR pulse generated from transform limited NIR light (taken from Fig. 4). Color lines: spectra of the MIR pulses obtained for different NIR pulse delays, normalized to their relative intensity.

In summary, we reported on the generation of narrowbandwidth CEP-stable MIR pulses in the mid-infrared wavelength range between 10 and 15 μm (20–30 THz) by DFG between chirped NIR pulses. The technique allowed us to easily reduce the MIR bandwidth by inserting highly dispersive ZnSe rod pairs in the NIR beam paths. We generated MIR pulses with bandwidths down to 1.6% $\Delta\omega/\omega_0$, a MV/cm peak electric field, and a good time-bandwidth product. These pulses were tunable by delaying the chirped NIR pulses with respect to each other. We expect these pulses to find important applications in the coherent vibrational control of solids.

Funding. European Union's Horizon 2020 Research and Innovation programme (654148); Laserlab-Europe.

REFERENCES

1. M. Först, R. Mankowsky, and A. Cavalleri, Acc. Chem. Res. **48**, 380 (2015).
2. R. Mankowsky, M. Först, and A. Cavalleri, Rep. Prog. Phys. **79**, 64503 (2016).
3. M. Först, C. Manzoni, S. Kaiser, Y. Tomioka, Y. Tokura, R. Merlin, and A. Cavalleri, Nat. Phys. **7**, 854 (2011).
4. T. F. Nova, A. Cartella, A. Cantaluppi, M. Först, D. Bossini, R. V. Mikhaylovskiy, A. V. Kimel, R. Merlin, and A. Cavalleri, Nat. Phys. AOP (2016), doi: 10.1038/nphys3925.
5. A. Sell, A. Leitenstorfer, and R. Huber, Opt. Lett. **33**, 2767 (2008).
6. R. A. Kaindl, M. Wurm, K. Reimann, P. Hamm, A. M. Weiner, and M. Woerner, J. Opt. Soc. Am. **17**, 2086 (2000).
7. D. W. McCamant, P. Kukura, S. Yoon, and R. A. Mathies, Rev. Sci. Instrum. **75**, 4971 (2004).
8. F. Raoult, A. C. L. Boscheron, D. Husson, C. Sauteret, A. Modena, V. Malka, F. Dorchies, and A. Migus, Opt. Lett. **23**, 1117 (1998).
9. G. Veitas and R. Danielius, J. Opt. Soc. Am. B **16**, 1561 (1999).
10. S. Wandel, M.-W. Lin, Y. Yin, G. Xu, and I. Jovanovic, J. Opt. Soc. Am. B **33**, 1580 (2016).
11. F. O. Koller, K. Haiser, M. Huber, T. E. Schrader, N. Regner, W. J. Schreier, and W. Zinth, Opt. Lett. **32**, 3339 (2007).
12. J. R. Danielson, A. D. Jameson, J. L. Tomaino, H. Hui, J. D. Wetzel, Y. S. Lee, and K. L. Vodopyanov, J. Appl. Phys. **104**, 033111 (2008).
13. R. Singla, G. Cotugno, S. Kaiser, M. Först, M. Mitrano, H. Y. Liu, A. Cartella, C. Manzoni, H. Okamoto, T. Hasegawa, S. R. Clark, D. Jaksch, and A. Cavalleri, Phys. Rev. Lett. **115**, 187401 (2015).
14. S. Rajasekaran, E. Casandruc, Y. Laplace, D. Nicoletti, G. D. Gu, S. R. Clark, D. Jaksch, and A. Cavalleri, Nat. Phys. **12**, 1012 (2016).
15. K.-H. Hong, J.-H. Kim, Y. H. Kang, and C. H. Nam, Appl. Phys. B **74**, s231 (2002).
16. G. Cerullo, A. Baltuška, O. D. Mücke, and C. Vozzi, Laser Photon. Rev. **5**, 323 (2011).
17. C. Manzoni, M. Först, H. Ehrke, and A. Cavalleri, Opt. Lett. **35**, 757 (2010).
18. A. Baltuška, T. Fuji, and T. Kobayashi, Phys. Rev. Lett. **88**, 133901 (2002).
19. C. Manzoni, D. Polli, and G. Cerullo, Rev. Sci. Instrum. **77**, 023103 (2006).
20. B. Tatian, Appl. Opt. **23**, 4477 (1984).
21. N. P. Barnes and M. S. Piltch, J. Opt. Soc. Am. **67**, 628 (1977).
22. M. Bass, *Handbook of Optics*, 3rd ed., Vol. **IV** of Optical Properties of Materials, Nonlinear Optics, Quantum Optics (McGraw-Hill, 2009).
23. A. A. Said, M. Sheik-Bahae, D. J. Hagan, T. H. Wei, J. Wang, J. Young, and E. W. Van Stryland, J. Opt. Soc. Am. B **9**, 405 (1992).
24. R. Trebino, *Frequency-Resolved Optical Gating: The Measurement of Ultrashort Laser Pulses* (Kluwer Academic, 2000).
25. B. Liu, H. Bromberger, A. Cartella, T. Gebert, M. Först, and A. Cavalleri, Opt. Lett. **42**, 129 (2017).